Numerical Simulation of Silicon Heterojunction Solar Cells Featuring Metal Oxides as Carrier-Selective Contacts

Christoph Messmer, Martin Bivour, Jonas Schön, Stefan W. Glunz, Martin Hermle

Abstract— **The applicability of different high (low) work function contact materials for the formation of alternative passivating and hole (electron) selective contacts is currently re-explored for silicon solar cells. To assist the engineering of those contacts which is still in its infancy, numerical device simulations are used to improve knowledge regarding relevant hetero-junction and thin film properties with the focus on metal oxide based hole contacts. The importance of (i) a high metal oxide work function for the induced c-Si pn-junction is shown. It is elucidated that for an efficient hole transport from this induced c-Si junction into the external electrode, via the buffer and the metal oxide, (ii) the metal oxide´s conduction band must be below the valence band of the buffer (or c-Si absorber) for direct band-to-band tunneling, or (iii) bulk traps near the valence band edge of the buffer (or c-Si absorber) are needed for trap-assisted tunneling.**

Index Terms—**Heterojunctions, Simulation, Fundamentals, Inversion-layer, Amorphous silicon, Selectivity, Band-to-band tunneling, Trap-assisted tunneling**

I. Introduction

Passivating and carrier-selective contacts [1] have the potential to overcome some of the intrinsic efficiency limitations of the established homojunction contact schemes. For the latter, doping of the silicon surface region is applied to obtain carrier-selective device regions below the unpassivated metal electrodes. The high recombination in this region is linked to a high dark saturation current J_0 and therefore results in moderate voltage at MPP and open-circuit conditions. Both passivating and non-passivating carrier-selective contacts typically obey the diode model described by the Shockley equations:

$$\boldsymbol{J = J_{gen} - J_0 \{\exp[q\, V/(n\, k_B T)] - 1\}} \qquad (1)$$

where q is the elementary charge, n the ideality factor and k_B the Boltzmann constant. One important assumption for Eq. (1) is that the voltage (V), which corresponds to the quasi-Fermi level splitting within the absorber at the edge of the pn-junction, equals the external voltage ($V_{external}$) at the contacts. The quasi-Fermi level splitting can also be expressed by the implied voltage ($V_{implied}$). The assumption $V_{external} = V_{implied}$ is typically fulfilled for a negligible gradient in the majority carrier quasi-Fermi level in the contact region. This means that low-injection conditions in the contact region during operation must be maintained [2], i.e. that the majority carrier density remains well above the minority carrier density ($n_{maj} \gg n_{min}$). Or, in a more general expression, that the conductivity σ of majority carrier remains well above those of the minority carriers ($\sigma_{maj} = q\, \mu_{maj}\, n_{maj} \gg \sigma_{min} = q\, \mu_{min}\, n_{min}$, μ is the mobility) [3]. Basically, we define contacts to be "selective" for which $V_{external} = V_{implied}$ and hence the validity of the diode equation are fulfilled. Accordingly, we define contacts to be "non-selective" when having a significant voltage loss in the contact region during operation leading to $V_{external} < V_{implied}$.

Similar to classical homojunctions, for TOPCon [4] and poly-Si [5] related contacts obtaining carrier selectivity is typically not the main design constraint. This is explained by the high doping efficiency of the partly crystalline silicon thin films and the c-Si wafer surface. It ensures that the majority carrier density in the contact region during equilibrium ($n_{maj,0}$) is already much higher than the excess carrier density that will be added during operation ($\Delta n = \Delta p$). Accordingly,

$$n_{maj} = n_{maj,0} + \Delta p \gg n_{min} = n_{min,0} + \Delta n$$

with $\Delta n \gg n_{min,0}$, is typically fulfilled. For TOPCon and poly-Si related contacts, an intermediate passivating dielectric buffer (SiO_x) ensures that those contacts are not only selective but also passivating. Accordingly, J_0 is low and the device characteristic and the limiting losses are well described by the diode equation.

The application of different high (low) work function thin films for the formation of passivating and hole (electron) selective contacts is another currently explored approach for silicon solar cells. So far, most promising candidates are transition metal oxide based heterojunctions leading to efficiencies up to 22 % [6–10]. However, other materials are also under investigation [11]. Work in this field can be understood as a renaissance of the induced silicon junctions (e.g. metal-insulator-semiconductor) from the 1970´s [12] by taking advantage of (i) novel or better studied high (low) work function contact materials mainly adapted from organic elec-tronics [13] and (ii) improvements of the passivating interme-diate buffer layers (a-Si:H, ultrathin dielectrics). However, knowledge regarding relevant junction and material properties and their engineering, stability issues and the integration of those high (low) work function contact materials in the c-Si solar cell device architectures is still in its infancy. Basically, engineering towards sufficient selectivity seems to be of more importance compared to devices featuring n- and p-type doped carrier-selective silicon regions.

The authors are with the Fraunhofer Institute for Solar Energy Systems (ISE), Freiburg, Germany (e-mail: christoph.messmer@ise.fraunhofer.de). Jonas Schön and Stefan Glunz are also with the Department of Sustainable Systems Engineering (INATECH), Albert-Ludwigs-Universität Freiburg 79110, Germany

Within this work the operation principles, important design parameters and losses of contact schemes based on induced junctions are reviewed with the help of numerical device simulations. The importance of the induced c-Si dark band bending, the voltage loss in the contact region, the band line-up and an efficient tunneling transport are addressed.

II. Simulation Method

All simulations in this paper are carried out using Sentaurus Device which allows the implementation of various models necessary for modelling hetero devices [14].

A. Simulation Setup

Since the investigated devices have no lateral distinction simulations are carried out in (quasi-)1D. The silicon bulk is n-type and the electron contact on the rear side is idealized and the same for all structures featuring a layer of intrinsic amorphous silicon a-Si(i):H and n-type a-Si(n) [Parameters listed in the appendix, Table II]. However, the focus will be on the p-contact at the front side featuring a passivating buffer layer and a high work function wide band gap metal oxide. We will approach this final contact system step-by-step by analyzing the following structures:

(a) The simplest contact is a metal-semiconductor contact (**MS**) with an induced pn-junction described by the Schottky model [14]. The equilibrium band diagram of such a contact is shown in Fig. 1a and the highly hole populated and inverted c-Si surface can be seen. There are two important parameters to set for this simple contact:

(i) The work function of the metal-like layer Φ^{metal} determining the built-in potential of the c-Si part of the induced junction. The latter corresponds to the band bending φ^{cSi} in the crystalline silicon. Note, that for this simulation study we don't speak of vacuum work functions as listed in literature but always of an 'effective work function' after contacting which takes Fermi-level pinning into account. Still, all the simulation results can be compared to experimental data by using φ^{cSi} as a figure of merit which can be easily measured by SPV measurements.

(ii) The surface recombination velocity S_0^{metal} which in this case is set to $10\,\text{cm/s}$ mimicking a good chemical surface passivation of the metal/c-Si. Note that MS contacts in reality form highly defective interfaces so that S_0^{metal} is much higher. However, this MS contact with 'artificially' lowered S_0^{metal} is still useful to distinguish between phenomena arising from this simple induced junction and those from the more complex structures (b) and (c).

(b) The next step to approach a more realistic contact is to add a passivating buffer layer – in our case 5 nm thick undoped amorphous silicon. We get a **MIS**-like structure (see Fig. 1b) where the buffer decouples S_0^{metal} from the junction recombination. S_0^{metal} is set to 10^6 cm/s for all the following structures. As can be seen, the induced band bending is shared by the buffer and the c-Si surface. Hence, φ^{cSi} is reduced to some extend but the c-Si is still highly inverted. We get a heterojunction between a-Si and c-Si which usually has small defect concentrations at the interface, thus we set the surface recombination velocity S_0^{cSi} to zero, unless stated otherwise.

(c) Finally, we add a transition metal oxide (TMO) like 10 nm thick layer with a high band gap of 3 eV and a variable work function Φ^{TMO} and bulk defect density (see Fig. 1c). For simplicity and referring to the standard silicon hetero junction (SHJ) featuring p-type a-Si instead of the high work function TMO, we will call this hole contact Transition metal oxide based SHJ (**T-SHJ**). The TMO / a-Si:H contact adds a second heterojunction and in principle two tunneling paths which are essential for the contact to work: Path (I) is direct band-to-band tunneling (B2B) from the valence band of the buffer to the conduction band of the TMO (see Fig. 1c). For path (II)

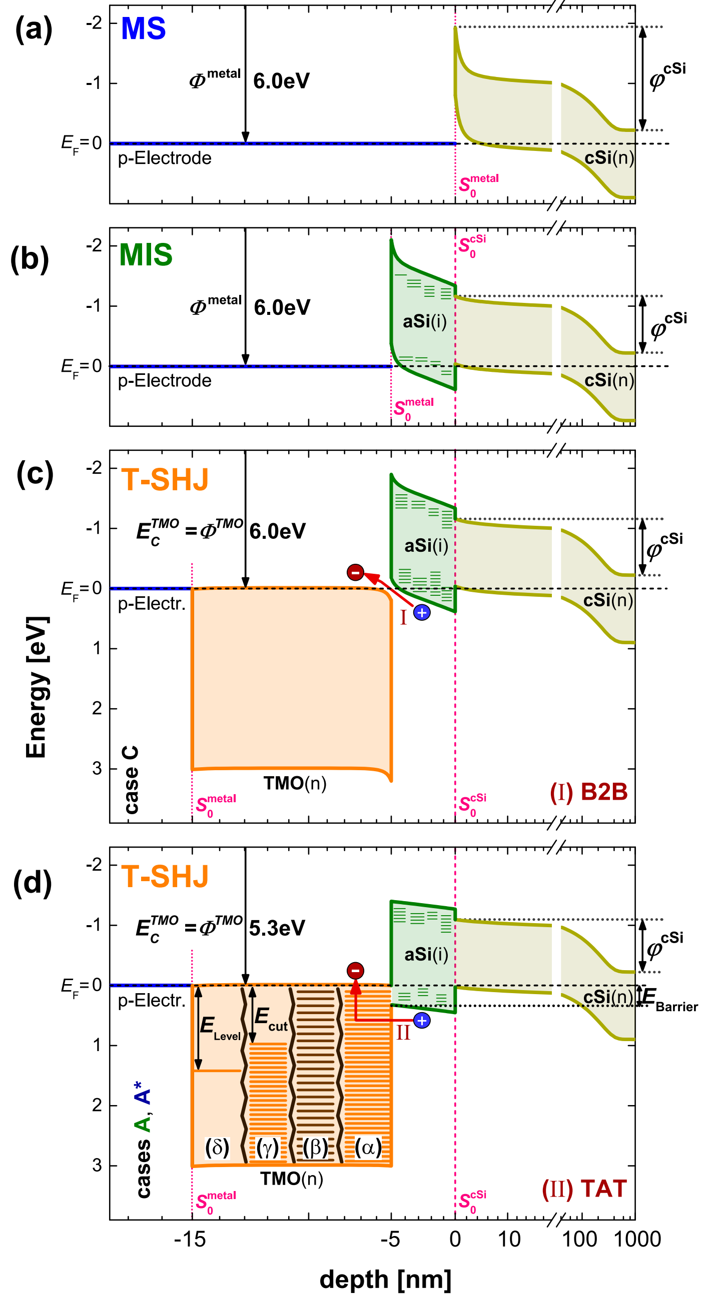

Fig. 1: Band diagrams of the three investigated p-contacts in the dark: **(a)** MS – Metal-Silicon **(b)** MIS – with additional intrinsic amorphous Si-layer **(c)** T-SHJ – Transition metal oxide Silicon Hetero Junction, B2B path (case C) **(d)** T-SHJ for a lower work function with Trap-Assisted Tunneling. (case A, A*) Four different TMO trap distributions (α-δ) are schematically shown.

traps in the band gap of the TMO provide an additional transport path, i.e. trap-assisted tunneling (TAT, see Fig. 1d) [14]. How we modelled the defect traps within the TMO is described in the next section.

B. *Modelling of the traps within the TMO*

As will be shown the density and the energetic distribution of the traps inside the TMO band gap greatly affect the TAT current. First some general notes on how the traps are modelled in this paper:

The TMO has a thickness of 10 nm and is n-type doped in a way that its work function equals the TMO conduction band energy $\Phi^{\mathrm{TMO}}=E_C^{\mathrm{TMO}}$ as shown in Fig. 1d (n-doping concentration: 10^{20} cm^{-3}). The traps are implemented electrically neutrally (that means we put half donor traps and half acceptor traps in the TMO) in order to just influence the tunneling current. Furthermore, the traps are in all cases implemented spatially uniform throughout the TMO.

In this paper we will consider four different distributions (α)-(δ) of the traps which we try to visualize in Fig. 1d and describe in the following:

(α) The energetic distribution of the traps is uniform throughout the whole bandgap with a very high density of $\rho_{\mathrm{Traps}}^{\mathrm{TMO}}=10^{20}$ cm^{-3} (which is equal to the n-doping concentration). Therefore, we will call this case "metallic" or "metal-like" since the defect distribution within the TMO provides energy states through the whole band gap. In this case we can assume that the TAT is not limiting the current of the cell.

(β) This case is like (α), i.e. we still have a uniform energy distribution of the traps, but we lower the trap density $\rho_{\mathrm{Traps}}^{\mathrm{TMO}}$ by orders of magnitude down to values like 10^{11} cm^{-3}.

(γ) To investigate the influence of the traps close to the conduction band of the TMO, starting from (α) we define an additional cut-off energy E_{cut} (depicted in Fig. 1d). Between the conduction band of the TMO-like layer and this energy all traps are omitted, therefore the first available energy level lies at $E=\Phi^{\mathrm{TMO}}+E_{\mathrm{cut}}$. (Note: The overall trap density is therefore getting smaller for higher E_{cut}, whereas the trap density per energy is still equal to that of (α)).

(δ) Some further investigations are carried out by a single defect level. This level has an energy E_{Level} with respect to the conduction band of the TMO and a density of $\rho_{\mathrm{Level}}^{\mathrm{TMO}}=10^{20}$ cm^{-3}.

III. SIMULATION RESULTS

In this chapter we aim to separate the different basic requirements needed to build a hole-selective contact step-by-step. In the first section we will present a simple showcase to discuss the importance of the induced c-Si junction and to clarify what we mean by non-ideal selectivity. We will show how it can be quantified and distinguished from other phenomena like classical losses as described by the diode model where ideal selectivity is linked to a proper rectifying i.e. diode-like contact characteristic. Section B will compare the influence of the work function on the structures presented in section II.A, while section C will investigate the influence of the tunneling transport for the T-SHJ structure.

A. *Importance of induced c-Si junction: Non-ideal selectivity*

Let us first consider the three different T-SHJ hole contacts listed in Table 1. Contact A has a sufficiently high work function (Φ=5.3 eV) exceeding the valance band energy of the c-Si absorber (5.19 eV) and no c-Si surface recombination (S_0^{cSi}=0) and is therefore solely limited by Auger recombination (ideal case). Furthermore, we constructed two cases A*

			external			internal		
Contact	Φ [eV]	S_0^{cSi} [cm/s]	j_{sc} [mA/cm²]	FF [%]	V_{oc} [mV]	iV_{oc} [mV]	ΔV [mV]	φ^{cSi} [meV]
A	5.3	0	42.2	88	740	740	0	870
A*	5.3	$5.3\cdot10^{6}$	41.6	82	574	578	4	870
B	5.0	0	42.0	82	574	707	133	701

Table 1: Three different hole contacts with their external and internal characteristics: (A) intrinsic Auger limit (A*) limited by high surface recombination S_0^{cSi} (B) limited by work function $\boldsymbol{\Phi}$.

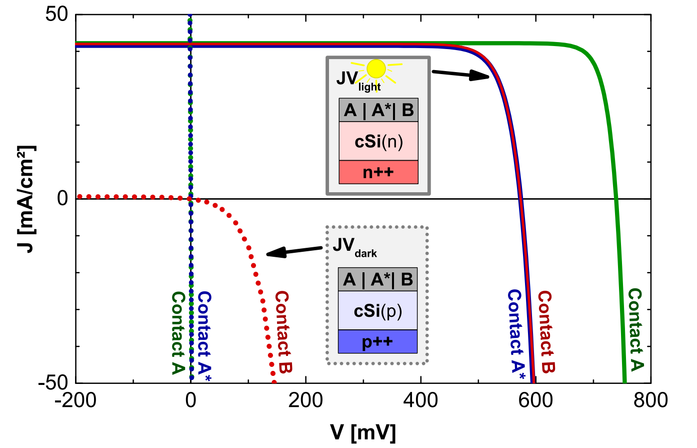

Fig. 2: JV-curves for the contacts listed in Table 1. Solid lines show the characteristics for one sun on an n-type bulk, dotted lines show the dark characteristics on a p-type bulk.

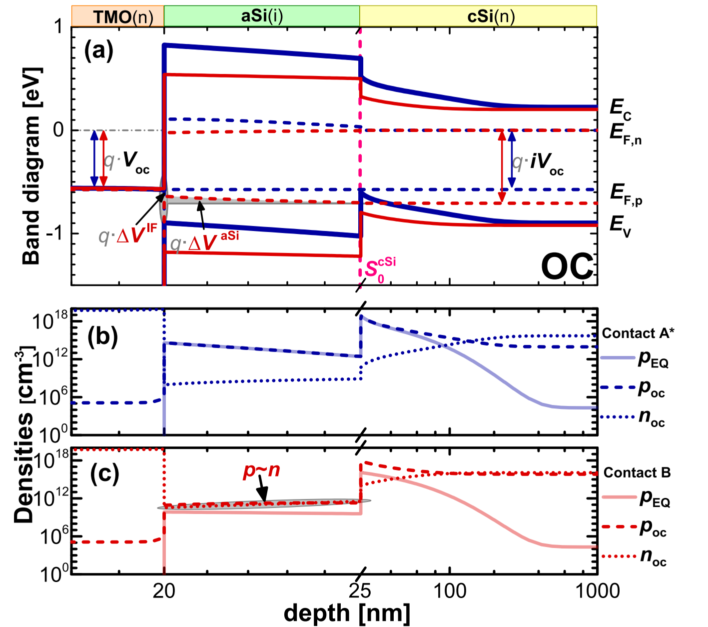

Fig. 3: (a) Band diagram of contact A* and B (Table 1) at open-circuit conditions. (b, c) Hole and electron densities at open-circuit (p_{oc}, n_{oc}) and hole density at equilibrium (p_{EQ}) for contact A* (blue) and B (red)

and B in a way that contact A* has the same high work function but no surface passivation (i.e. high S_0^{cSi}) – Contact B is well-passivated (S_0^{cSi}=0) but its work function is not sufficiently high (Φ=5.0 eV). (For all of these three contacts tunneling is ideal, i.e. distribution (α) was used.)

If we look at the JV_{light}-curves (Fig. 2, solid line) for an experimentally typical range and the external cell parameters (Table 1) we notice no significant distinction of the two curves of contact A* (blue) and B (red) although their power losses arise from different phenomena. For a better loss analysis we want to discuss three quantities, namely the implied open-circuit voltage (iV_{oc}), the difference of the iV_{oc} and external V_{oc} (ΔV) and the inversion of the c-Si surface during equilibrium which is quantified by the induced c-Si band bending (φ^{cSi}). These "internal" cell parameters, given in Table 1, are depicted in a band diagram in Fig. 3a and can be extracted experimentally with little effort [15].

Starting with $\boldsymbol{\varphi^{\mathrm{cSi}}}$**:** For contact A* the band bending φ^{cSi} is the same as for contact A since the work function is the same (see Table 1). However, the work function of contact B is too low to form a proper pn-junction which results in a φ^{cSi} which is 169 meV lower. Basically, φ^{cSi} increases the local hole density in the contact region with respect to the c-Si bulk as shown in Fig. 3b,c (p_{EQ}, solid line) during equilibrium. Accordingly, the asymmetry of the hole/electron conductivity in this device region is also increased which is the decisive parameter for obtaining the selective extraction of excess holes from the absorber [3, 16], i.e. a proper rectifying and diode-like carrier transport. Although φ^{cSi} describes this asymmetry only in the dark it is directly related to the asymmetry during operation when excess electrons and holes are generated by the same amount ($p/n = (p_0 + \Delta p)/(n_0 + \Delta n)$) [3]. Accordingly, the influence of φ^{cSi} can also be seen during operation at MPP and open-circuit (OC) conditions. For the latter this is shown in Fig. 3b,c. For the high work function of contact A* (Fig. 3b) this asymmetry is maintained during operation since p_{oc} (dashed lines) is well above n_{oc} (dotted lines) in the contact region. For the low work function of contact B this asymmetry cannot be maintained during operation, i.e. $p{\sim}n$ in the contact region (see Fig. 3c). The latter is accompanied by a significant gradient in the majority carrier Fermi-level and voltage loss (ΔV) in the contact region as highlighted in grey in Fig. 3a. It violates one important boundary condition of the standard pn-junction theory [2]. Accordingly, such contacts and their losses are not properly described by standard diode equation.

$\boldsymbol{iV_{\mathrm{oc}}}$**:** Owing to the lack of chemical passivation the iV_{oc} of contact A* shows a significant drop to 578 mV whereas the iV_{oc} of contact B is above 700 mV. This difference can be directly seen in the band diagram at OC where the iV_{oc} equals the splitting of the hole and electron quasi Fermi levels in the bulk of the absorber (Fig. 3a, right dashed lines).

$\boldsymbol{\Delta V_{oc} = iV_{oc} - V_{oc}}$**:** This difference between internal and external voltage results from the gradient in the majority carrier Fermi-level in the contact region and is significant for contact B ($\Delta V \gg 0$), whereas for contact A* it is negligible. The origin of this voltage loss ΔV for contact B is due to $p \sim n$ (see Fig. 3c) in the contact region which lowers the hole conductivity σ_{h}. According to $j_{\mathrm{h}} = \sigma_{\mathrm{h}}\,\mathrm{grad}[E_{\mathrm{F,p}}]/q$ [3, 16], to drive a certain hole current density j_{h} through the p-contact a reduction of the hole conductivity σ_{h} has to come along with a higher gradient in the hole quasi Fermi level $E_{\mathrm{F,p}}$, i.e. a voltage loss ΔV. In our example this voltage loss of contact B is split up into ΔV^{aSi} = 67 mV within the amorphous silicon (visible fermi level gradient in Fig. 3a) and ΔV^{IF} = 66 mV at the TMO/a-Si interface (not directly visible).

Since voltage losses ΔV arise from non-ideal selectivity we will use ΔV as a figure of merit for selectivity losses. However, it should be noted that besides ΔV another experimental method to probe insufficient selectivity of a contact is to measure the dark JV-curve for the contact put on an absorber with inverse doping (p-type) and a low resistive ohmic rear contact. In this case an identical and low-ohmic characteristic is obtained for high work function contacts A and A* which is mainly limited by the absorber resistivity (see Fig. 2, dotted $\mathrm{JV_{dark}}$). For contact B a poor hole selectivity is obtained for the p-type absorber, reflected in a diode-like characteristic.

We conclude: While contact A* is limited due to classical recombination losses, contact B is limited by an insufficient work function Φ and hence insufficient asymmetry of the conductivities leading to a selectivity loss ΔV in the contact region during operation. It should be noted that similar conditions are also obtained at MPP.

More generally, we have seen that a high iV_{oc} is linked to a good c-Si surface passivation and a low ΔV indicates ideal selectivity. For the latter a high work function Φ is needed to get a high c-Si band bending φ^{cSi} and thus to maintain the asymmetric p/n conductivity in the contact region during operation.

B. *Influence of the work function*

This section discusses the influence of the work function for the p-contacts introduced in chapter II (Fig. 1) step-by-step.

(a) Metal-Silicon (MS)

The results for the metal-semiconductor interface are shown in Fig. 4 (in blue). The dark blue curve in in Fig. 4a shows the efficiency for the hole contact introduced in Fig. 1a (p-contact on an n-type c-Si bulk) while the light blue curve shows the efficiency for an electron contact (n-contact on a p-type c-Si bulk), both as a function of the work function Φ of the metal.

The two curves are symmetric around the mid gap energy of c-Si $E_{\mathrm{midgap}}^{\mathrm{cSi}} \approx$ 4.63 eV. For the hole (electron) contact the efficiency reaches a maximum of $\eta = 28\%$ for a work function Φ greater (smaller) than the valence (conduction) band energy E_V^{cSi} ≈5.19 eV (E_C^{cSi} ≈4.07 eV). Getting closer to the region of the c-Si mid-gap energy the efficiency drops and then decreases linearly until it reaches zero. Therefore, a sufficiently high (low) work function is the first condition for building a good hole (electron) selective contact since it modifies the asymmetry of the conductivity as motived before.

To analyze where these power losses come from we will have a closer look at the open-circuit (OC) voltage of the cell, shown in Fig. 4b. For the hole contact with a work function

above the valence band energy of c-Si ($\Phi > E_V^{\text{cSi}}$) the curves of iV_{oc} (dotted blue line) and the V_{oc} (solid blue line) match, therefore ΔV=0 which indicates an ideal selectivity of the contact. In this range the V_{oc} is solely limited by the intrinsic limit (Auger recombination) comparable to the case of contact A in section III, A.

If the work function is lower than the valence band energy of c-Si ($\Phi < E_V^{\text{cSi}}$) the V_{oc} drops while the iV_{oc} stays above 728 mV. The latter indicates that the mimicked 'passivation' at the metal/c-Si interface is very good (S_0^{metal}=10 cm/s). However, the external voltage V_{oc} drops for decreasing work functions in a linear fashion [17–19]. A similar behavior is obtained for *FF* and j_{sc} (not shown). The difference between iV_{oc} and V_{oc} per definition leads to $\Delta V > 0$ and indicates that the losses in voltage (and efficiency) are due to non-ideal selectivity of the contact (similar to contact B in section III,A).

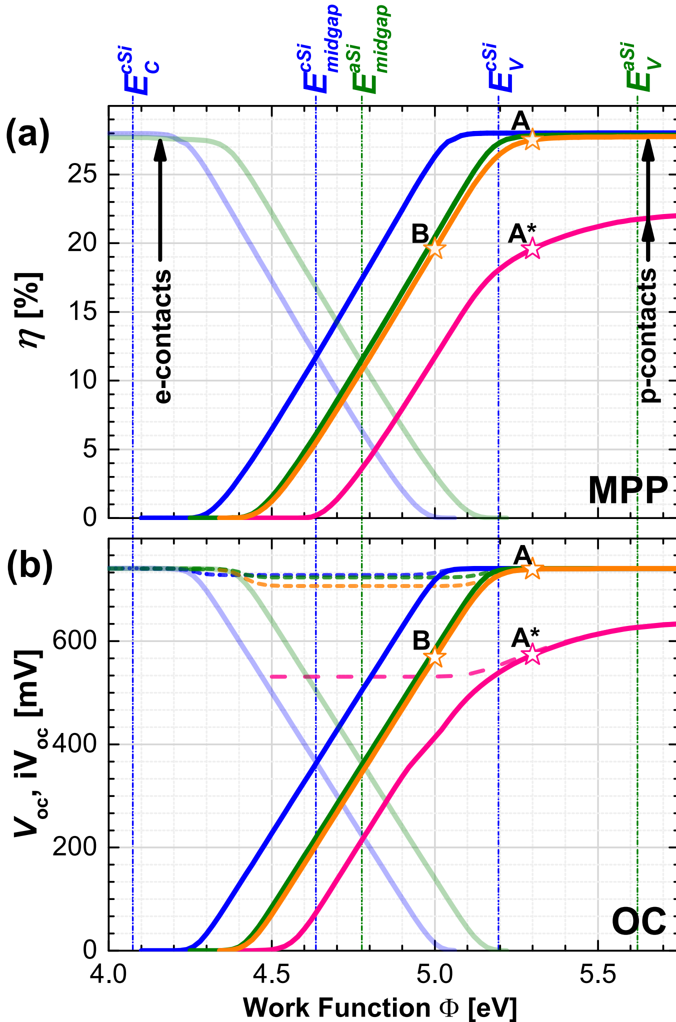

Fig. 4: **(a)** Efficiency η, **(b)** V_{oc} and iV_{oc} as a function of the metal/TMO work function Φ for the three different p-contact systems of Fig. 1. For MS and MIS, the light-colored curves show the mirrored n-contact. The p-contact for T-SHJ is shown for two different surface passivations S_0^{cSi} (orange and pink) and the three cases A, A* and B (of chapter III.A) are highlighted.

(b) Metal-iLayer-Silicon (MIS)

When adding 5 nm of intrinsic amorphous silicon between the metal and the c-Si bulk, which for real devices is needed for a good surface passivation, we get the MIS-like structure shown in Fig. 1b and the characteristic shown in Fig. 4, green.

Both the efficiency η and the open-circuit voltages V_{oc} and iV_{oc} show the same characteristic as for the MS structure, except that they are shifted by 0.15 eV to higher work functions. Whereas the MS curves were symmetric around the mid-gap energy of c-Si, the green curves are centered about the mid-gap energy of a-Si $E_{\text{midgap}}^{\text{aSi}} \approx$4.78 eV. This raises the demand on the TMO work function Φ in order to reach a high c-Si band bending φ^{cSi}, but still a work function Φ slightly greater than the c-Si valence band energy E_V^{cSi} is sufficient to reach a high φ^{cSi} and therefore maximum efficiency.

Like for the MS structure the V_{oc} around the mid-gap energy shows the well-known linear behavior [17, 20] with a slope of 1 V/eV which indicates that for this range the work function Φ shows a one-to-one relation with respect to the limiting built-in voltage of the contact and therefore the c-Si band-bending φ^{cSi}[3, 19].

(c) TMO Silicon Hetero Junction (T-SHJ)

In this last step we add the high-band gap, n-type Transition Metal Oxide (TMO) layer with a high trap density inside its band gap and hence another heterojunction to obtain the TMO / a-Si:H(i) / c-Si p-contact introduced in Fig. 1c,d.

Let us first consider the results shown in orange (Fig. 4). We see that the T-SHJ contact in this case shows a similar behavior with respect to efficiency and voltage (also fill factor and j_{sc}) as the MIS-like structure, despite its higher complexity due to tunneling at the TMO/a-Si interface. The reason for this is that we modelled the TMO in a way that it behaves "metal-like" (distribution (α) in chapter II,B). This means that the hole extraction from the inverted c-Si region towards the external electrode is based on an efficient tunneling via the TMO gap states. The influence of the distribution of these gap states will be discussed in the next subsection.

For the sake of completeness Fig. 4 shows a T-SHJ contact with poor chemical surface passivation (S_0^{cSi}=5.3·10^6 cm/s, pink) resulting in a lower iV_{oc} and hence lower efficiency. However, for higher work functions ΔV=0 indicates ideal selectivity despite the poor chemical passivation. The iV_{oc} stays above 531 mV for work functions around the mid-gap of a-Si while the V_{oc} drops further due to insufficient c-Si band-bending φ^{cSi}.

Note that the three p-contacts A, A* and B (discussed in section III,A) are highlighted in Fig. 4 to relate back to section A and emphasize once more the difference between power losses due to an insufficient work function (case B) and power losses due to a poor chemical passivation (case A*).

We conclude that the T-SHJ structure behaves like a MIS-like structure as long as the TMO electrically behaves like a metal. However, it is important to understand what happens if the tunneling at the TMO interface has a limiting influence. The next section will discuss some cases.

C. Transport limitations at the TMO/a-Si interface

In the last section we assumed the transport via tunneling at the TMO/a-Si interface to be non-limiting. However, for real cells there might be complex and non-metal-like distributions of the defect traps which are subject of this section. In Fig. 5 the cell characteristics for different trap concentrations are shown as a function of Φ^{TMO}.

Let us first concentrate on the efficiency η (Fig. 5d). The MIS-like structure (green), the T-SHJ structure of Fig. 4 (light orange, solid line) and the former discussed cases A, B, and C (see Fig. 1c) are plotted as references reflecting only the power losses caused by an insufficient work function. The other data provide information on the TMO properties namely the traps and their distribution. An important TMO/a-Si heterojunction property is the position of the TMO conduction band with respect to the valence band of the a-Si:H buffer which we define as $E_{\mathrm{Barrier}} = E_V^{\mathrm{aSi}} - E_C^{\mathrm{TMO}}$ (see Fig. 1d). We plot this as a second x-axis in Fig. 5. It should be highlighted again that for simplicity reasons $E_C^{\mathrm{TMO}} \equiv \Phi^{\mathrm{TMO}}$ for the TMO is assumed here.

All curves match for $E_{\mathrm{Barrier}} < 0$ ($E_C^{\mathrm{TMO}} > E_V^{\mathrm{aSi}}$). This is because a TMO conduction band energy greater than the a-Si valance band energy allows an efficient transport at the TMO / a-Si:H contact by Band-To-Band Tunneling (B2B) independent of the TMO traps (see Fig. 1c).

However, if $E_{\mathrm{Barrier}} > 0$ ($E_C^{\mathrm{TMO}} < E_V^{\mathrm{aSi}}$) the TMO conduction band energy is lower than the valence band energy of the a-Si layer (shown in Fig. 1d), an efficient Trap-Assisted Tunneling (TAT) is needed. Thus, the efficiency crucially depends on the TMO traps. When lowering the density $\rho_{\mathrm{Traps}}^{\mathrm{TMO}}$ of the homogeneously distributed traps we see that the efficiency decreases (see β in Fig. 5d, orange to black lines). This effect is less pronounced for higher work functions Φ. Accordingly, lower traps densities come along with higher demands on the work function. Assuming an ideal TAT transport a work function larger than 5.2 eV is needed to reach the maximum efficiency.

The influence of the energetic trap distribution within the TMO band gap (see γ in Fig. 1d) is shown by different dotted orange lines in Fig. 5d: There is a general loss in efficiency the more we cut-off energy levels close to the conduction band of the TMO. The *FF* limitation for the non-metal like cases is depicted in Fig. 5c. For decreasing trap densities, we get an overall drop of the fill factor except for $E_{\mathrm{Barrier}} < 0$ ($\Phi > E_V^{\mathrm{aSi}}$) where B2B-Tunneling is efficient. The dotted *FF* curves for increasing cut-off energies E_{cut} match the metal-like case (solid orange line) for low work functions. But as the work function increases the fill factor reaches its maximum and drops again for higher work functions.

To understand the influence of E_{cut} we have to understand the contribution of different energetic levels within the TMO

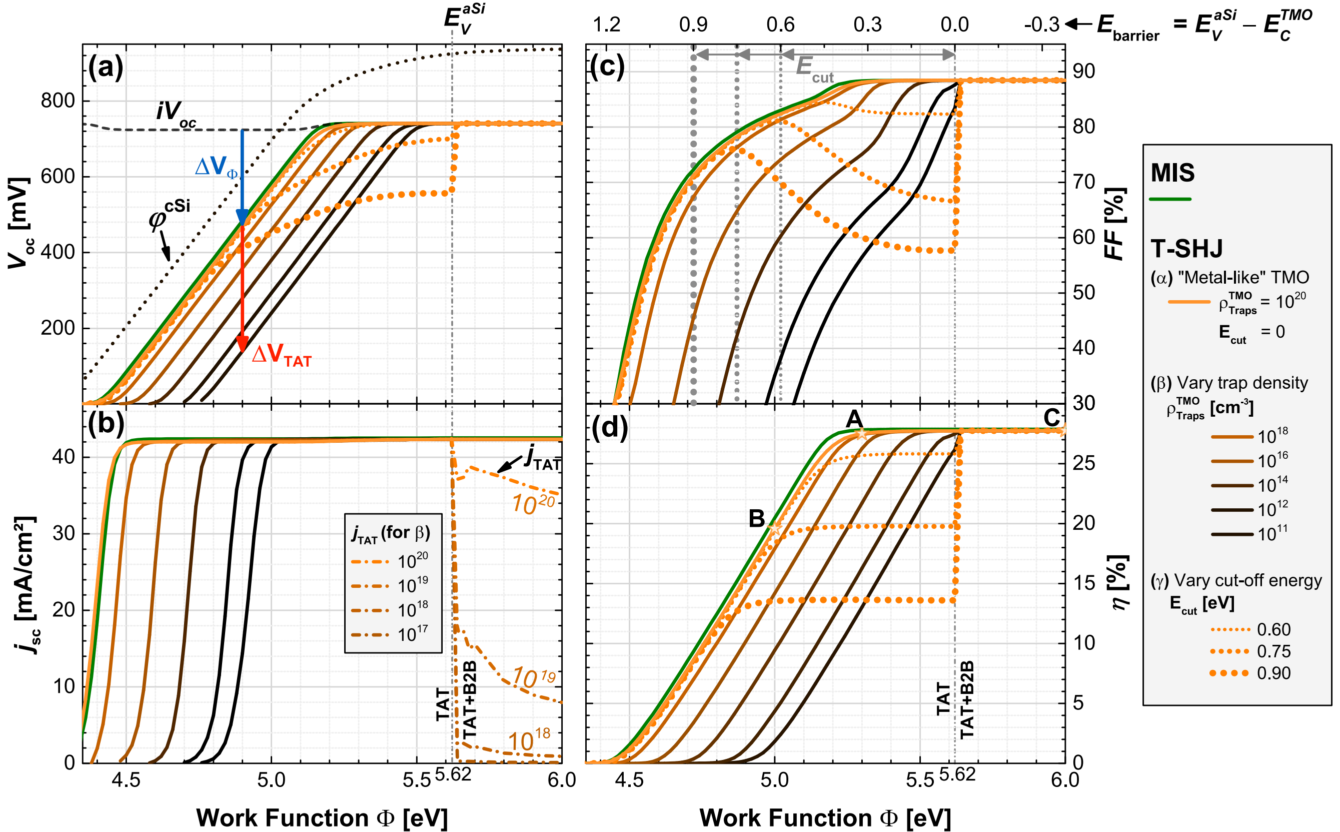

Fig. 5: (a) Open-circuit voltage V_{oc} (b) short-circuit current j_{sc} (c) fill factor *FF* and (d) efficiency η as a function of the TMO work function Φ for different trap distributions (α-γ introduced in II.B). The MIS-like structure and the "metal-like" T-SHJ of Fig. 4 are plotted as references (in green and light orange). (β) shows variation of the uniformly distributed trap density as solid lines in different shades of orange. (γ) shows variation of $\boldsymbol{E}_{\mathrm{cut}}$ as dotted lines in orange. (a) additionally shows the c-Si band-bending $\boldsymbol{\varphi}^{\mathrm{cSi}}$ and iV_{oc} (same for all curves) and selectivity losses ΔV_Φ, ΔV_{TAT} due to insufficient work function (blue arrow) and insufficient TAT tunneling (red arrow), respectively. (b) additionally shows the Trap-assisted Tunneling current $\boldsymbol{j}_{\mathrm{TAT}}$ (dash-dotted) (c) additionally shows the cut-off energies in grey (d) highlights the cases A (see Fig. 1d and III.A) and B (see III.A) and C (see Fig. 1c).

bandgap. Therefore, we placed a single trap level at energy E_{Level} and varied its energetic position inside the TMO band gap (variation δ in Fig. 1d). Let us consider the green curve in Fig. 6a which shows the fill factor of the T-SHJ structure as a function of E_{Level} for a TMO work function and conduction band energy of Φ=5 eV and the corresponding equilibrium band diagram. One can see that the fill factor is poor (<20%) and therefore transport is inefficient for E_{Level} between zero and E_{Barrier}, which means for a trap between the conduction band energy of the TMO and the valance band energy of the a-Si:H buffer. For a trap level E_{Level} slightly larger than E_{Barrier} we get efficient transport since holes in the a-Si valence band are now able to reach the TMO defect level. However, the further we increase E_{Level} the fewer holes can reach the defect level and contribute to the transport. This is explained by their thermal energy which is not sufficient. For even higher E_{Level}, e.g. the TMO mid gap energy no significant transport is observed. This shows that for an efficient TAT transport, the traps close to the a-Si valence band are of most importance. (Note, that we only considered *elastic* TAT which doesn't include phonon interactions [21]. However, for phonon energies greater than zero the *FF* onset would be smoother including energies between E_V^{aSi} and E_C^{TMO}.)

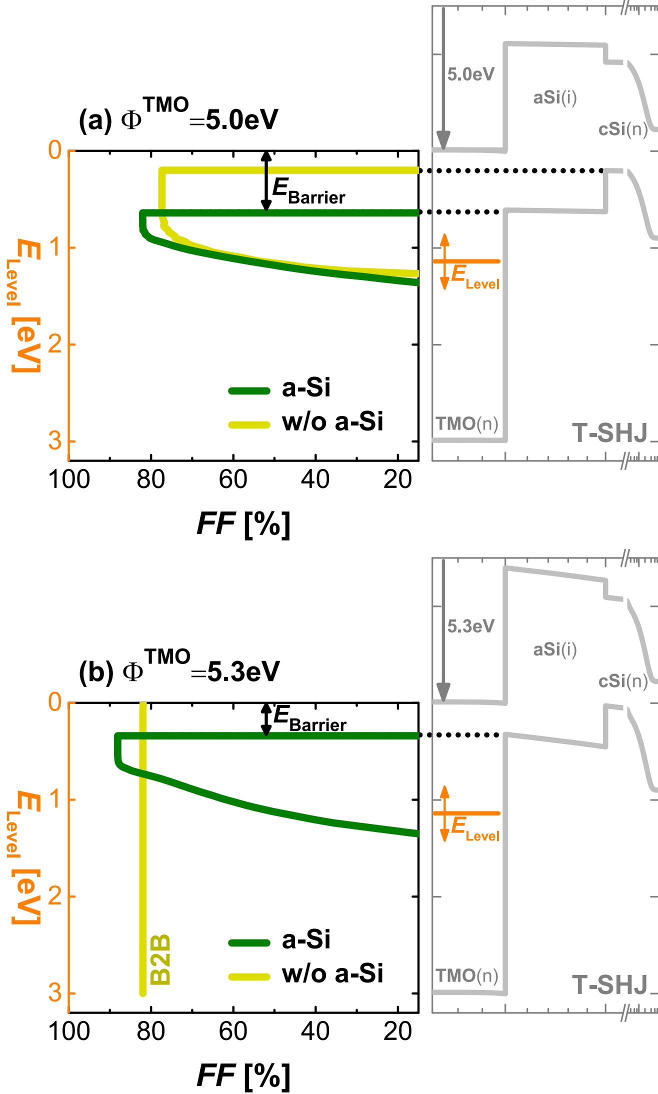

Fig. 6: Fill factor *FF* as a function of the energy $\boldsymbol{E}_{\mathrm{Level}}$ of a single trap level within the TMO bandgap (variation δ in Fig. 1) for (a) Φ=5eV and (b) Φ=5.3eV and corresponding equilibrium band diagram. The green curves correspond to the *FF* of the T-SHJ structure, whereas the yellow curves correspond to the T-SHJ structure without a-Si(i) passivation layer for which the TMO is in direct contact with the c-Si. For the latter the equilibrium band diagrams are not shown.

However, considering the case that the a-Si buffer layer is omitted (yellow curve in Fig. 6a, band diagram not shown) the traps close the c-Si valence band are of most importance and efficient tunneling is shifted by 0.45 eV to lower E_{Level}. This shift corresponds to the a-Si/c-Si valence band offset. This suggests that without buffer, traps closer to the TMO conduction band and with buffer traps further way from E_C^{TMO} are needed for an efficient TAT. The *FF* for around mid-gap energies is hardly affected since for these energetic locations it is the mean thermal energy of the charge carriers which is decisive for the transport (and is unchanged). However, Fig. 6b shows that omitting the buffer can further change the requirements on the provided tunneling paths: The green curve in Fig. 6b shows the T-SHJ with a-Si for a higher TMO work function of Φ=5.3 eV compared to Fig. 6a. This lowers E_{Barrier} by $\Delta\Phi$=0.3 eV. It means that traps closer to the TMO conduction band are needed for a high *FF*. Without buffer (yellow curve) E_{Barrier} becomes negative for the higher work function of the TMO which allows for B2B tunneling and traps are not needed for an efficient transport. This shows that the actual band alignment defines the requirements on the traps inside the TMO and if traps are needed at all.

Going back to Fig. 5c, this finding helps to understand the behavior of the fill factor when varying the trap distribution near the TMO conduction band (γ, dotted lines). For $E_{\mathrm{barrier}}>E_{\mathrm{cut}}$ the dotted curves match the metal-like TMO (solid orange curve). This is because it makes no difference if we cut-off traps with energy $E<E_{\mathrm{barrier}}$, since they do not contribute to the transport. However, if we increase the TMO work function Φ^{TMO} and therefore decrease E_{barrier} to $E_{\mathrm{barrier}}<E_{\mathrm{cut}}$, the omitted energy levels move into the energy region close to the a-Si valence band energy. This leads to a fill factor loss. The further we increase Φ (i.e. decrease E_{barrier}), the fewer holes thermally reach the available energy levels at $E>E_{\mathrm{cut}}$. However, for $E_{\mathrm{barrier}}<0$, B2B-Tunneling sets in leading to a fill factor which is independent of the traps. Accordingly, a sharp *FF* increase is observed for Φ^{TMO} (i.e. E_C^{TMO}) close to the a-Si valence band energy of 5.62 eV.

Fig. 5b shows that the short-circuit conditions are least affected by an inefficient hole transport. High short-circuit currents j_{sc} are obtained while for OC and MPP there are already significant losses. The graph also highlights that for $E_C^{\mathrm{TMO}}<E_V^{\mathrm{aSi}}$ the total current is driven only by TAT ($j_{\mathrm{sc}}=j_{\mathrm{TAT}}$) while for $E_C^{\mathrm{TMO}}>E_V^{\mathrm{aSi}}$ it is driven by two parallel currents $j_{\mathrm{sc}}=j_{\mathrm{TAT}}+j_{\mathrm{B2B}}$ corresponding to the paths of TAT and B2B.

Finally, we address the open-circuit conditions in Fig. 5a which shows V_{oc}, iV_{oc} and c-Si band bending φ^{cSi} during equilibrium. First of all the c-Si band-bending φ^{cSi} is the same for all curves (black dotted curve) reflecting that the TMO trap distributions (α)-(γ) have no influence on φ^{cSi}. Furthermore,

the iV_{oc} (depicted as black dashed line) is similar for all curves and stays above 700 mV which indicates that the losses in V_{oc} are not due to a poor surface passivation, but due to selectivity losses reflected in $\Delta V>0$. Fig. 5a shows that there are two kinds of selectivity losses ΔV_{Φ}, ΔV_{TAT} that are exemplarily shown by the blue and the red arrow, respectively, and will be described in the next section.

D. Analysis of selectivity losses

Fig. 7 represents the simulation data of Fig. 5a by plotting the selectivity losses ΔV as a function of the c-Si band bending φ^{cSi}, which can be measured by SPV and takes Fermi-level pinning into account. The bottom right-hand corner corresponds to an ideal contact characteristic featuring a high c-Si band bending and no selectivity losses. For these well-selective contacts, the established characterization via ohmic contact and standard recombination losses as quantified by R_S and J_0 is a meaningful procedure since the diode equation is valid as motivated in section I. However, for novel contact schemes a prior classification in terms of Fig. 7 can be helpful for contact evaluation. Furthermore, Fig. 7 helps to distinguish two different kinds of selectivity losses:

(a) Selectivity losses ΔV_{Φ} due to insufficient work function
As already observed for the simple induced MS junction, an insufficient work function leads to an insufficient c-Si band bending which violates the asymmetric conductivities in the contact region. This leads to selectivity losses ΔV_{Φ} like shown in Fig. 7 (blue arrow) and highlights once more that a sufficiently high band bending is an essential requirement for good selectivity. Such a one-to-one relation of ΔV_{Φ} on φ^{cSi} (blue shaded area with slope -1) is due to the Schottky equation and has already been observed experimentally for metal [19], doped a-Si:H [15, 22] and metal oxide based contacts [22–25].

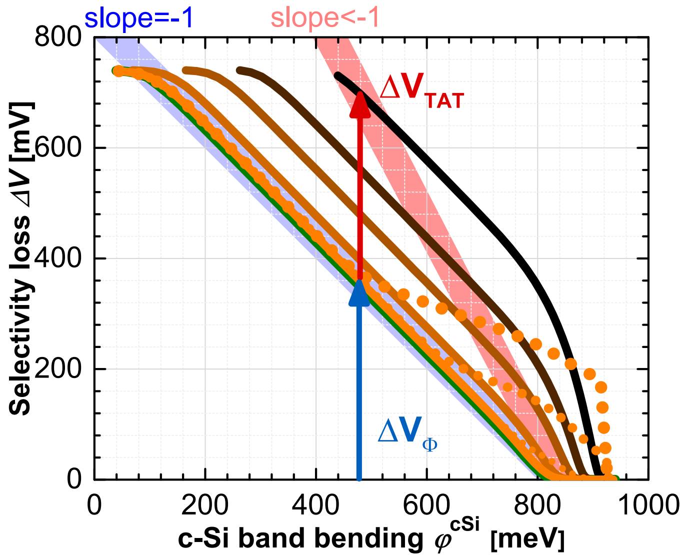

Fig. 7: Selectivity loss $\Delta V_{oc}=iV_{oc}-V_{oc}$ as a function of the c-Si band bending φ^{cSi}. The blue shaded area with slope -1 corresponds to selectivity losses ΔV_{Φ} only due to insufficient work function (exemplarily shown as blue arrow), whereas the red shaded area with a slope smaller than -1 shows additional selectivity losses ΔV_{TAT} due to insufficient TAT tunneling transport (exemplarily shown as red arrow).

(b) Selectivity losses ΔV_{TAT} due to insufficient tunneling
A major finding of this paper is that inefficient TAT tunneling leads to additional selectivity losses ΔV_{TAT} (exemplarily shown by the red arrow in Fig. 7). Therefore, selectivity problems (i.e. $\Delta V>0$) do not only arise from insufficient band bending (i.e. work function), as described in (a), but can also arise from insufficient tunneling transport due to absence of defects. This should be taken into account when experimental data is evaluated, since it might give further insight in the origin of selectivity losses, especially when the slope of Fig. 7 deviates from -1 (like e.g. for the red shaded area).

Whether or not insufficient tunneling plays a decisive role in an actual device is subject to further investigations. A first comparison with experiments was drawn in [22, 26], leading to promising agreement of the simulations of this paper and experimental data both qualitatively and quantitatively.

IV. Conclusion

A fundamental understanding of carrier-selective contacts featuring metal oxides was generated. This supports the search for suitable materials and improves the interpretation of experimental data. This is especially true when using ΔV (the difference between internal and external voltage which is linked to a gradient of the majority quasi Fermi level in the contact region) as a figure of merit for the contacts selectivity. We modeled a transition metal oxide based silicon heterojunction featuring a high band gap n-type metal oxide to form a hole-selective contact. We deduced the following guidelines to build a hole-selective contact (similar findings should apply for electron contacts):

(i). The induced hole density in the contact region, quantified by the band bending φ^{cSi}, has to be sufficiently high. This is the case for a TMO work function Φ close to the valence band energy of the absorber. However, a passivating buffer layer (e.g. a-Si) is expected to further raise the demand on the TMO work function.

$$\Phi \gtrsim E_V^{\mathrm{cSi}} \quad \Rightarrow \ \varphi^{\mathrm{cSi}} \text{ sufficiently high}$$

(ii). A TMO conduction band energy E_C^{TMO} greater than the valence band energy of the buffer E_V^{aSi} (or, if omitted, the absorber E_V^{cSi}) allows for band-to-band tunneling of excess holes.

$$E_C^{\mathrm{TMO}} > E_V^{\mathrm{aSi}} \quad \Rightarrow \ \mathrm{B2B}$$

(iii). If (ii) is not fulfilled an efficient hole transport via trap-assisted tunneling by traps in the TMO close to the valence band energy of the buffer (absorber) is needed.

$$E_C^{\mathrm{TMO}} < E_V^{\mathrm{aSi}} \quad \Rightarrow \ \mathrm{TAT}$$

An important finding for experimental investigations is that both an insufficient work function *and* inefficient tunneling (e.g. due to absence of traps) can cause insufficient selectivity (i.e. $\Delta V > 0$) resulting in power losses. Taking the guidelines from above into account allows to minimize those losses by engineering the contact towards better selectivity. Only after that, once the external voltage matches the internal voltage, the diode equation is valid and the well-established optimization of 'classical' losses like ohmic contact resistivity and passivation, quantified by R_S and J_0, is a meaningful procedure.

ACKNOWLEDGMENT

This work was funded by the European Project "DISC" under the European Union's Horizon 2020 Research and Innovation Program under grant agreement N°727529, and by the German Federal Ministry for Economic Affairs and Energy under contract N°0324141 "SELEKTIV".

V. REFERENCES

[1] R. M. Swanson, "Approaching the 29% limit efficiency of silicon solar cells," in *31st IEEE Photovoltaic Specialists Conference Lake Buena Vista*, Lake Buena Vista, FL, USA, 2005, pp. 889–894.

[2] S. M. Sze, *Physics of semiconductor devices,* 2nd ed. New York: John Wiley & Sons, 1981.

[3] P. Würfel and U. Würfel, *Physics of solar cells: From basic principles to advanced concepts,* 3rd ed. Weinheim: Wiley-VCH, 2016.

[4] F. Feldmann, M. Bivour, C. Reichel, M. Hermle, and S. W. Glunz, "Passivated rear contacts for high-efficiency n-type Si solar cells providing high interface passivation quality and excellent transport characteristics," *Sol. Energy Mater. Sol. Cells*, vol. 120, pp. 270–274, 2014.

[5] R. Peibst, U. Romer, Y. Larionova, H. Schulte-Huxel, T. Ohrdes, M. Haberle, B. Lim, J. Krugener, D. Stichtenoth, T. Wutherich, C. Schollhorn, J. Graff, and R. Brendel, "Building blocks for back-junction back-contacted cells and modules with ion-implanted poly-Si junctions," in *40th IEEE Photovoltaic Specialists Conference Denver*, Denver, CO, USA, 2014, pp. 852–856.

[6] J. Geissbühler, J. Werner, S. Martin de Nicolas, L. Barraud, A. Hessler-Wyser, M. Despeisse, S. Nicolay, A. Tomasi, B. Niesen, and S. de Wolf, "22.5% efficient silicon heterojunction solar cell with molybdenum oxide hole collector," *Applied Physics Letters*, vol. 107, no. 8, p. 81601, 2015.

[7] X. Yang, Q. Bi, H. Ali, K. Davis, W. V. Schoenfeld, and K. Weber, "High-performance TiO_2-based electron-selective contacts for crystalline silicon solar cells," (eng), *Advanced Materials*, vol. 28, no. 28, pp. 5891–5897, 2016.

[8] M. Mews, L. Korte, and B. Rech, "Oxygen vacancies in tungsten oxide and their influence on tungsten oxide/silicon heterojunction solar cells," *Solar Energy Materials and Solar Cells*, vol. 158, pp. 77–83, 2016.

[9] L. G. Gerling, S. Mahato, A. Morales-Vilches, G. Masmitja, P. Ortega, C. Voz, R. Alcubilla, and J. Puigdollers, "Transition metal oxides as hole-selective contacts in silicon heterojunctions solar cells," *Solar Energy Materials and Solar Cells*, vol. 145, pp. 109–115, 2016.

[10] M. Bivour, J. Temmler, H. Steinkemper, and M. Hermle, "Molybdenum and tungsten oxide: High work function wide band gap contact materials for hole selective contacts of silicon solar cells," *Sol. Energy Mater. Sol. Cells*, vol. 142, pp. 34–41, 2015.

[11] J. Bullock, Y. Wan, M. Hettick, J. Geissbühler, A. J. Ong, D. Kiriya, Di Yan, T. Allen, J. Peng, X. Zhang, and others, "Survey of dopant-free carrier-selective contacts for silicon solar cells," in *Photovoltaic Specialists Conference (PVSC), 2016 IEEE 43rd*, 2016, pp. 210–214.

[12] R. Singh, M. A. Green, and K. Rajkanan, "Review of conductor-insulator-semiconductor (CIS) solar cells," *Solar Cells*, vol. 3, no. 2, pp. 95–148, 1981.

[13] L.-M. Chen, Z. Xu, Z. Hong, and Y. Yang, "Interface investigation and engineering – achieving high performance polymer photovoltaic devices," *J. Mater. Chem.*, vol. 20, no. 13, p. 2575, 2010.

[14] Synopsis, "Sentaurus Device User Guide: release L-2016.03-SP2," http://www.synopsys.com, 2016.

[15] M. Bivour, M. Reusch, S. Schroer, F. Feldmann, J. Temmler, H. Steinkemper, and M. Hermle, "Doped layer optimization for silicon heterojunctions by injection-level-dependent open-circuit voltage measurements," *IEEE J. Photovoltaics*, vol. 4, no. 2, pp. 566–574, 2014.

[16] U. Würfel, A. Cuevas, and P. Würfel, "Charge carrier separation in solar cells," *IEEE Journal of Photovoltaics*, vol. 5, no. 1, pp. 461–469, 2015.

[17] W. Schottky, "Vereinfachte und erweiterte Theorie der Randschicht-gleichrichter," *Zeitschrift für Physik A Hadrons and Nuclei*, vol. 118, no. 9, pp. 539–592, 1942.

[18] H. Steinkemper, "Numerical Simulation of Silicon Solar Cells," Dissertation, Universität Konstanz, Konstanz, 2017.

[19] M. Bivour, "Silicon heterojunction solar cells analysis and basic understanding," Dissertation, Fraunhofer ISE, Albert-Ludwigs-Universität Freiburg, Freiburg im Breisgau, 2015.

[20] M. A. Green and J. Shewchun, "Minority carrier effects upon the small signal and steady-state properties of Schottky diodes," *Solid-State Electronics*, vol. 16, no. 10, pp. 1141–1150, 1973.

[21] F. Jiménez-Molinos, A. Palma, F. Gamiz, J. Banqueri, and J. A. Lopez-Villanueva, "Physical model for trap-assisted inelastic tunneling in metal-oxide-semiconductor structures," *Journal of Applied Physics*, vol. 90, no. 7, pp. 3396–3404, 2001.

[22] M. Bivour, C. Messmer, L. Neusel, F. Zähringer, J. Schön, S. Glunz, and M. Hermle, "Principles of Carrier-selective Contacts based on Induced Junctions: Presented at the 33rd European PV Solar Energy Conference and Exhibition, 25-29 September 2017, Amsterdam, The Netherlands," Fraunhofer Institute for Solar Energy Systems (ISE), 2017.

[23] M. Bivour, B. Macco, J. Temmler, W. E.M. Kessels, and M. Hermle, "Atomic layer deposited molybdenum oxide for the hole-selective contact of silicon solar cells," *Energy Procedia*, vol. 92, pp. 443–449, 2016.

[24] L. Neusel, M. Bivour, and M. Hermle, "Selectivity issues of MoOx based hole contacts: Energy Procedia," 2017.

[25] M. Bivour, F. Zähringer, P. Ndione, and M. Hermle, "Sputter-deposited WOx and MoOx for hole selective contacts: Energy Procedia," 2017.

[26] C. Messmer, "Numerical Simulation and Analysis of Metal Oxide Contact Properties for Silicon Heterojunction Solar Cells," Master thesis, Albert-Ludwigs-Universität Freiburg, 2017.

TABLE II
SIMULATION PARAMETERS

Symbol	Quantity	Value
	Sentaurus	
	Version	L-2016.03-SP2
	Global	
	Temperature	300 K
	Spectrum	AM1.5, 1 sun
	TMO	
	Thickness	10 nm
	Band gap	3 eV
	Donor concentration	10^{20} cm^{-3}
$\rho_{\mathrm{Traps}}^{\mathrm{TMO}}$	Trap concentration	varied
	Trap volume	10^{-6} µm³
	Trap capture cross section (eXSection, hXSection)	10^{-12} cm²
	Amorphous silicon (a-Si)	
	Thickness	5 nm
	Crystalline silicon (c-Si)	
	Thickness	150 µm
	Resistivity	1 Ωcm (n-type for p-contact p-type for n-contact)
	Rear	
	a-Si(i) thickness	5 nm
	a-Si(doped) thickness	10 nm
	a-Si(doped) doping conc.	10^{21} cm^{-3} (n-type for p-contact p-type for n-contact)
	Interfaces	
S_0^{metal}	Recombination velocity at metal	10^1 cm/s for MS 10^6 cm/s for MIS, T-SHJ
S_0^{cSi}	Recombination velocity at c-Si interface	0 cm/s for MIS, T-SHJ
	Tunneling	
	e-, h-Tunneling masses	0.1
	g factors	1
	TAT-Tunneling	Elastic (E_{Phonon}=0)
	Models	
	Auger model	Standard ("Auger", [11])